PERGAMON

International Journal of Heat and Mass Transfer 45 (2002) 1865–1877

International Journal of HEAT and MASS TRANSFER

www.elsevier.com/locate/ijhmt

Temperature solution in multi-dimensional multi-layer bodies

A. Haji-Sheikh [a,*], J.V. Beck [b]

[a] *Department of Mechanical and Aerospace Engineering, The University of Texas at Arlington, 500 West First Street, Arlington, TX 76019-0023, USA*

[b] *Department of Mechanical Engineering, Michigan State University, East Lansing, MI 48824-1226, USA*

Received 12 April 2001; received in revised form 23 August 2001

Abstract

Mathematical steps leading to computation of the temperature field in multi-dimensional, multi-layer bodies are described and numerical results for two-layer bodies are presented. The presentations include boundary conditions of the first, second, and third kind. Included in this paper is a table to assist in computing eigenvalues. Also, modifications are made to account for the contribution of contact resistance. An efficient computational scheme for calculating the eigenvalues is discussed and numerical results are presented. For multi-dimensional, multi-layer bodies, the eigenfunctions may have real or imaginary eigenvalues. The complete solution must include the contribution of imaginary eigenvalues; otherwise, the information will be erroneous. A procedure is introduced that places a bound on the location of each eigenvalue.

Keywords: Transient; Analysis; Heat conduction; Multi-dimensional; Layered materials

1. Introduction

Although most industrial problems in transient heat conduction are solved using approximate numerical methods, the need exists for exact solutions. One of these needed areas is in three-dimensional composite layers. Analytical solutions can provide insight into the behavior of the temperature and heat flux distributions that are more difficult to obtain from the numerical solutions. Perhaps even more important are the emerging fields of verification and validation. Verification refers to the accurate solution of the known describing equations of a process; usually these are partial differential equations. In validation, the emphasis is upon determining if the prescribed equations actually describe the physical process being modeled. This paper is intended to provide exact analytical solutions for verification of some large numerical codes modeling fires and other complex processes. It is part of a larger study at Sandia National Laboratories. The problem considered herein is for the two-layer heat conduction problem in a parallelepiped.

Many of the earlier studies address thermal conduction in one-dimensional, multi-layer bodies. A literature survey revealed several works on analytical solutions of heat conduction problems in composite media. A one-dimensional orthogonal expansion for a composite medium was developed by Tittle [1]. Padovan [2] developed a generalized Sturm–Liouville procedure for composite and anisotropic domains in transient heat conduction problems. The integral transform technique as applied to the solution of heat conduction problems in composite media is included in [3, Chapter 14]. Salt [4,5] examined the transient temperature solution in a two-dimensional, isotropic-composite slab. Mikhailov and Ozisik [6] analyzed the three-dimensional form of the problem published by Salt [4]. Yan et al. [7] worked on exact series solutions for three-dimensional temperature distributions in two-layer bodies subject to various types of boundary conditions. The numerical steps leading to one-dimensional temperature solutions in a two-layer body is reported in [8]. In general, basic steps leading to computation of temperature are widely available in the

* Corresponding author. Tel.: +1-817-272-2010; fax: +1-817-272-2952.

E-mail address: haji@mae.uta.edu (A. Haji-Sheikh).

0017-9310/02/$ - see front matter
PII: S0017-9310(01)00279-4

Nomenclature

a, b, c, d	dimensions in Fig. 1 (cm)
A, B	constants, Region 1
A_{mn}	Fourier coefficients
Bi_1	$h_1 b/k_{1y}$ in Region 1
Bi_2	$h_2(c-b)/k_{2y}$ in Region 2
Bi_b	$1/R_b$
C, D	constants, Region 2
c_{pi}	specific heat in Region i (J/kg K)
$f(\lambda)$	a function of eigenvalue, λ
F_1, F_2	see Eqs. (19a) and (19b)
Fo	Fourier number ($=\alpha_1 t/b^2$)
g_i	volumetric heat source in region i (W/cm^3)
G_{ij}	Green's function
i, j	indices
k_{ix}	thermal conductivity in Region i along x (W/cm K)
k_{iy}	thermal conductivity in Region i along y (W/cm K)
k_{iz}	thermal conductivity in Region i along y (W/cm K)
m, n	indices in eigenfunctions
$N_{x,m}$	norms for x-direction
$N_{y,mnp}$	norms for y-direction
$N_{z,n}$	norms for z-direction
q	heat flux (W/m^2)
r_i	$(k_{ix}/k_{iy})^{1/2}$
R	contact resistance (m^2 K/W)
R_b	Rk_{1y}/b
R_c	$Rk_{2y}/(c-b)$
s_i	$\sqrt{k_{iz}/k_{iy}}$
t	time (s)
T_i	temperature in Regions i (K)
$U(x,t)$	auxiliary function in Example 1
V, W	functions in Example 2
x, y, z	coordinates (cm)
X	eigenfunction in x-direction
Y	eigenfunction in y-direction
Z	eigenfunction in z-direction

Greek symbols

α_{1y}	$k_{1y}/\rho_1 c_{p1}$, thermal diffusivity in Region 1 (cm^2/s)
α_{2y}	$k_{2y}/\rho_2 c_{p2}$ thermal diffusivity in Region 2 (cm^2/s)
β_m	eigenvalue for x-direction (cm^{-1})
γ_{mnp}	eigenvalue for y-direction in Region 1 (cm^{-1})
$\Gamma(t)$	a function in solution for t
ε	deviation, see Eq. (36)
η_{mnp}	eigenvalue for y-direction in Region 2 (cm^{-1})
λ_{mnp}	eigenvalue for time (s^{-1})
v_n	eigenvalue for z-direction (cm^{-1})
ρ_i	density of regions i (kg/cm^3)
τ	time variable (s)
Φ	a function in Example 1
Ψ	see Eq. (39b)

literature [3]. For the purpose of parameter estimation, Aviles-Ramos et al. [9] use a two-dimensional, two-layer solution with prescribed heat flux over all surfaces and report that it is necessary to retain all eigenvalues, real or imaginary, to satisfy the completeness criterion of the solution.

Computation of temperature in multi-dimensional, multi-layer bodies exhibits a few features that are not commonly observed when computing the temperature in homogeneous bodies. As stated in [9], the eigenvalues may become imaginary and, therefore, the corresponding eigenfunctions will have imaginary arguments. Also, care must be exercised when computing the eigenvalues since the spacing between successive eigenvalues changes between zero and a maximum value. This work includes a procedure to target a band within which only one eigenvalue will be located as reported in [10] and a hybrid root finding scheme [10] is then used to rapidly compute the numerical value of that specific eigenvalue with a desired accuracy. The imaginary eigenvalues can produce numerical instability as the number of terms in a series solution becomes large.

The temperature solutions presented in this paper are Green's function types of solutions. Tables are provided to assist in the formulation of Green's function solutions depending on the specific boundary conditions. The solutions obtained are equally valid when each layer has orthotropic properties. Also, the eigenfunctions and eigenconditions are modified to account for the contribution of contact resistance between layers.

2. Mathematical formulation

To describe the mathematical formulations, consideration is given to a three-dimensional, two-layer body depicted in Fig. 1. Analytical derivation for a temperature solution in a two-layer body is described. The two layers may be isotropic or orthotropic. The diffusion equation for the orthotropic Region 1 is

$$k_{1x}\frac{\partial^2 T_1}{\partial x^2}+k_{1y}\frac{\partial^2 T_1}{\partial y^2}+k_{1z}\frac{\partial^2 T_1}{\partial z^2}=\rho_1 c_{p1}\frac{\partial T_1}{\partial t} \quad (1a)$$

when $0 < y < b$,

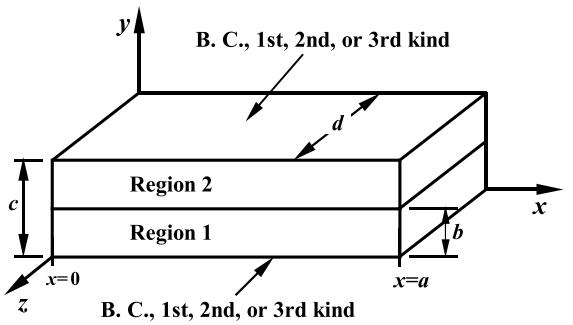

Fig. 1. Schematic of a three-dimensional two-layer body.

and in the orthotropic Region 2 is

$$k_{2x}\frac{\partial^2 T_2}{\partial x^2}+k_{2y}\frac{\partial^2 T_2}{\partial y^2}+k_{2z}\frac{\partial^2 T_2}{\partial z^2}=\rho_2 c_{p2}\frac{\partial T_2}{\partial t} \quad (1b)$$

when $b<y<c$.

2.1. Separation of variables

Assuming boundary conditions are homogeneous, one can propose solutions of the forms

$$T_1(x,y,z,t)=X_1(x)Y_1(y)Z_1(z)\Gamma_1(t) \quad \text{(in Region 1)} \quad (2a)$$

and

$$T_2(x,y,z,t)=X_2(x)Y_2(y)Z_2(z)\Gamma_2(t) \quad \text{(in Region 2)} \quad (2b)$$

satisfying the following conditions:

$$X_1''/X_1=X_2''/X_2=-\beta^2, \quad (3a)$$

$$Z_1''/Z_1=Z_2''/Z_2=-v^2, \quad (3b)$$

$$\Gamma_1'/\Gamma_1=\Gamma_2'/\Gamma_2=-\lambda^2, \quad (3c)$$

where β, v, and λ are constants depending on the specific type of homogeneous boundary conditions. Differential equations for Y_1 and Y_2 can be obtained following substitution of T_1 and T_2 in the appropriate forms of the diffusion equation:

$$\begin{aligned}-k_{1x}\beta^2+k_{1y}Y_1''/Y_1-k_{1z}v^2&=\rho_1 c_{p1}(-\lambda^2),\\ -k_{2x}\beta^2+k_{2y}Y_2''/Y_2-k_{2z}v^2&=\rho_2 c_{p2}(-\lambda^2),\end{aligned} \quad (4)$$

that yield

$$\begin{aligned}\frac{Y_1''}{Y_1}&=-\frac{\lambda^2}{\alpha_{1y}}+\frac{k_{1x}}{k_{1y}}\beta^2+\frac{k_{1z}}{k_{1y}}v^2=-\gamma^2,\\ \frac{Y_2''}{Y_2}&=-\frac{\lambda^2}{\alpha_{2y}}+\frac{k_{2x}}{k_{2y}}\beta^2+\frac{k_{2z}}{k_{2y}}v^2=-\eta^2,\end{aligned} \quad (5)$$

where $\alpha_{1y}=k_{1y}/\rho_1 c_{p1}$, $\alpha_{2y}=k_{2y}/\rho_2 c_{p2}$, $r_i=\sqrt{k_{ix}/k_{iy}}$, and $s_i=\sqrt{k_{iz}/k_{iy}}$ for $i=1$ or 2. The values of γ and λ are related to λ by the relations

$$\gamma^2=\lambda^2/\alpha_{1y}-(r_1^2\beta^2+s_1^2v^2), \quad (6a)$$

$$\eta^2=\lambda^2/\alpha_{2y}-(r_2^2\beta^2+s_2^2v^2). \quad (6b)$$

The temperature solutions T_1 and T_2, after replacing X by X_m, Z by Z_n, and Y by Y_{mnp}, leads to classical Fourier series solutions that take the following forms:

$$T_1=\sum_{p=1}^{\infty}\sum_{m=1}^{\infty}\sum_{n=1}^{\infty}A_{mnp}X_m(\beta_m x)Z_n(v_n z)Y_{1,mnp}(\gamma_{mnp}y)\times\exp(-\lambda_{mnp}^2 t), \quad (7a)$$

$$T_2=\sum_{p=1}^{\infty}\sum_{m=1}^{\infty}\sum_{n=1}^{\infty}A_{mnp}X_m(\beta_m x)Z_n(v_n z)Y_{2,mnp}(\eta_{mnp}y)\times\exp(-\lambda_{mnp}^2 t). \quad (7b)$$

The compatibility conditions are

$$T_1|_{y=b}+Rk_{1y}\partial T_1/\partial y|_{y=b}=T_2|_{y=b}, \quad (8a)$$

$$k_{1y}\partial T_1/\partial y|_{y=b}=k_{2y}\partial T_2/\partial y|_{y=b}, \quad (8b)$$

where R represents the contact resistance between the layers. This solution accepts the classical functions for X_m and Z_n subject to boundary conditions of the first kind and second kind in the x- and z-directions. It is to be emphasized that, for the x- and z-directions, only boundary conditions of the first kind and second kind are unconditionally admissible. However, at $y=0$ and at $y=c$, a boundary condition can be of the first, second, or third kind. For the sake of generality, the solution is cast in the form of a Green's function solution.

3. Green's function solution

In general, for all boundary conditions, Green's function using identities given in Beck et al. [11, Eqs. (10.56), (10.58), (10.68)], reduces to

$$G_{ij}(x,y,z,t|x',y',z',\tau)=\sum_{p=1}^{\infty}\sum_{m=1}^{\infty}\sum_{n=1}^{\infty}\frac{\rho_j c_{pj}X_m(x)X_m(x)Z_n(z)Z_n(z)Y_{i,mnp}(y)Y_{j,mnp}(y')}{N_{x,m}N_{y,mnp}N_{z,n}}\times\exp\lfloor-\lambda_{nnp}^2(t-\tau)\rfloor, \quad (9)$$

where $i=1,2,\ldots,M$; and $j=1,2,\ldots,M$, while M is the number of regions in the body. Eq. (9) describes the effect in region i due a pulse that appears at time τ in region j. The norms $N_{x,m}$, $N_{z,n}$, and $N_{y,mnp}$ are

$$N_{x,m}=\int_0^a[X_m(x)]^2\,dx, \quad (10)$$

$$N_{z,n} = \int_0^d [Z_n(z)]^2 \, \mathrm{d}z, \tag{11}$$

$$N_{y,mnp} = \int_0^b \rho_1 c_{p1} [Y_{1,mnp}(y)]^2 \, \mathrm{d}y + \int_b^c \rho_2 c_{p2} [Y_{2,mnp}(y)]^2 \, \mathrm{d}y. \tag{12}$$

The Green function solution in Region i is

$$\begin{aligned} T_i(\vec{r},t) = & \sum_{j=1}^{M} \int_{V_j} G_{ij}(\vec{r},t\,|\,\vec{r}',0) T_j(\vec{r}',0)\,\mathrm{d}V_j' \\ & + \sum_{j=1}^{M} \int_{\tau=0}^{t} \mathrm{d}\tau \int_{V_j} \frac{1}{\rho_j c_{pj}} G_{ij}(\vec{r},t\,|\,\vec{r}',\tau) g_j(\vec{r}',\tau)\,\mathrm{d}V_j' \\ & + \sum_{j=1}^{M} \int_{\tau=0}^{t} \mathrm{d}\tau \int_{S_j} \frac{k_j}{\rho_j c_{pj}} \left[G_{ij}(\vec{r},t\,|\,\vec{r}',\tau) \frac{\partial T(\vec{r}',\tau)}{\partial n} \right. \\ & \left. - T(\vec{r}',\tau) \frac{\partial G_{ij}(\vec{r},t\,|\,\vec{r}',\tau)}{\partial n} \right]_{S_j'} \mathrm{d}S_j', \end{aligned} \tag{13}$$

where $\mathrm{d}V' = \mathrm{d}x'\,\mathrm{d}y'\,\mathrm{d}z'$ and S_j' is a surface portion for the region j in prime space on which a boundary condition is specified. From this point forward, the computations are focused toward the solution of a two-layer body, $M = 2$. There are nine specific solutions depending on the boundary conditions over $y = 0$ and $y = c$ surfaces. All nine solutions can be obtained from a solution that uses boundary conditions of the third kind over $y = 0$ and $y = c$ surfaces.

As stated earlier, the contributions of Eqs. (3a) and (3b) to the temperature solution are limited to boundary conditions of the first kind and the second kind. The contribution of these boundary conditions over $x = 0, a$ and $z = 0, d$ surfaces are obtainable in a standard manner. The main task is to determine the solutions for Y_1 and Y_2 using Eq. (5). It is assumed that if the surfaces at $y = 0$ and $y = c$ are exposed to boundary conditions of the third kind; other linear boundary conditions can be deduced from that solution.

The solutions for Y_1 and Y_2, as given by Eq. (5) are

$$Y_1 = A\cos(\gamma y) + B\sin(\gamma y), \tag{14a}$$

$$Y_2 = C\cos(\eta y) + D\sin(\eta y). \tag{14b}$$

Eq. (14a) must satisfy the following condition at $y = 0$:

$$k_{1y} \frac{\partial Y_1}{\partial y}\bigg|_{y=0} = h_1 Y_1\Big|_{y=0}. \tag{15}$$

After substituting for Y_1 and $\partial Y_1/\partial y$, one obtains

$$A = \frac{k_{1y} B \gamma}{h_1} \quad \text{or} \quad B = \left(\frac{h_1}{k_{1y}}\right) A. \tag{16}$$

Next, one must satisfy the compatibility conditions at $y = b$, Eqs. (8a) and (8b), that is,

$$\begin{aligned} Y_1 &= \frac{k_{1y} B\gamma}{h_1} \cos(\gamma y) + B\sin(\gamma y) \\ &= B\left[\frac{k_{1y}\gamma}{h_1}\cos(\gamma y) + \sin(\gamma y)\right], \end{aligned} \tag{17}$$

$$\begin{aligned} &\left(\frac{C}{B}\right)\cos(\eta b) + \left(\frac{D}{B}\right)\sin(\eta b) = F_1, \\ &-\left(\frac{C}{B}\right)\sin(\eta b) + \left(\frac{D}{B}\right)\cos(\eta b) = F_2, \end{aligned} \tag{18}$$

where

$$\begin{aligned} F_1 = & \frac{k_{1y}\gamma}{h_1}\cos(\gamma b) + \sin(\gamma b) \\ & + Rk_{1y}\gamma\left[-\frac{k_{1y}\gamma}{h_1}\sin(\gamma b) + \cos(\gamma b)\right], \end{aligned} \tag{19a}$$

$$F_2 = \left(\frac{k_{1y}}{k_{2y}}\right)\left(\frac{\gamma}{\eta}\right)\left[-\frac{k_{1y}\gamma}{h_1}\sin(\gamma b) + \cos(\gamma b)\right]. \tag{19b}$$

The solutions for C/B and D/B are

$$\begin{aligned} \frac{D}{B} &= F_1\sin(\eta b) + F_2\cos(\eta b), \\ \frac{C}{B} &= F_1\cos(\eta b) - F_2\sin(\eta b). \end{aligned} \tag{20}$$

Next, using the boundary condition of the third kind at $y = c$,

$$-k_{2y}\frac{\partial Y_2}{\partial y}\bigg|_{y=c} = h_2 Y_2\big|_{y=c}$$

for Y_2 solution, taken from Eq. (14b), results in the relation

$$\begin{aligned} &-k_{2y}[-C\eta\sin(\eta y) + D\cos(\eta y)] \\ &\quad = h_2[C\cos(\eta y) + D\sin(\eta y)] \end{aligned}$$

or

$$\begin{aligned} &\frac{C}{B}\left[\sin(\eta c) - \frac{h_2}{k_{2y}\eta}\cos(\eta c)\right] - \frac{D}{B}\left[\cos(\eta c) + \frac{h_2}{k_{2y}\eta}\sin(\eta c)\right] \\ &\quad = 0. \end{aligned} \tag{21}$$

Replacing C/B and D/B, using Eqs. (19a), (19b), and (20), and after some algebraic steps, the eigencondition is

$$\begin{aligned} f(\lambda) = & \left\{\left[\frac{h_1 b}{k_{1y}} - \frac{Rk_{1y}}{b}(\gamma b)^2\right]\frac{\sin(\gamma b)}{\gamma b} + (1 + h_1 R)\cos(\gamma b)\right\} \\ & \times \left[[\eta(c-b)]\sin[\eta(c-b)] - \frac{h_2(c-b)}{k_{2y}}\cos[\eta(c-b)]\right] \\ & + \left(\frac{c-b}{b}\right)\left(\frac{k_{1y}}{k_{2y}}\right)\left[\cos[\eta(c-b)] + \frac{h_2(c-b)}{k_{2y}}\right. \\ & \left. \times \frac{\sin[\eta(c-b)]}{\eta(c-b)}\right]\left[(\gamma b)\sin(\gamma b) - \frac{h_1 b}{k_{1y}}\cos(\gamma b)\right] = 0, \end{aligned} \tag{22}$$

where γ and η are related to λ by Eqs. (6a) and (6b). The final form of the eigencondition after further simplification is

$$\frac{(h_2/k_{2y})-\eta\tan[\eta(c-b)]}{(h_2/k_{2y})\tan[\eta(c-b)]+\eta} = -\left(\frac{k_{1y}}{k_{2y}}\right)\left(\frac{\gamma}{\eta}\right)\frac{h_1/k_{1y}-\gamma\tan(\gamma b)}{(h_1/k_{1y}-Rk_{1y}\gamma^2)\tan(\gamma b)+\gamma(1+Rh_1)}. \tag{23a}$$

One can obtain an alternative form for Eq. (23a) if the quantity $k_{1y}\partial T_1/\partial y$ in Eq. (8a) is replace, using Eq. (8b), by $k_{2y}\partial T_2/\partial y$; that is,

$$\frac{(h_2/k_{2y})-\eta\tan[\eta(c-b)]}{(h_2/k_{2y}-Rk_{2y}\eta^2)\tan[\eta(c-b)]+\eta(1+Rh_2)} = -\left(\frac{k_{1y}}{k_{2y}}\right)\left(\frac{\gamma}{\eta}\right)\frac{h_1/k_{1y}-\gamma\tan(\gamma b)}{(h_1/k_{1y})\tan(\gamma b)+\gamma}. \tag{23b}$$

The functions Y_1 and Y_2, as well as the eigencondition, Eq. (23a) or (23b), can be extended to include the effect of boundary conditions of the first kind, as $h_i\to\infty$, and the second kind, as $h_i\to 0$, at surfaces $y=0$ and/or $y=c$. This task is accomplished and the coefficients A, B, C, and D needed to construct eigenfunctions are summarized in Table 1(a). Each entry YIJ refers to the boundary condition of the Ith kind at $y=0$ and Jth kind at $y=c$. Therefore, each entry is for a specific boundary condition at $y=0$ and a boundary condition of the first, second, or third kind at $y=c$. For a convective boundary condition at $y=0$, the values of B, C, and D are selected using $A=1$. For convenience of this presentation and subsequent computations, it is convenient to combine Eqs. (14b), (19a), (19b), and (20) to get

$$Y_2=\bar{C}\cos[\eta(y-b)]+\bar{D}\sin[\eta(y-b)]. \tag{24}$$

The coefficients $\bar{C}$ and $\bar{D}$ that correspond to coefficients A and B are listed in Table 1(b). The eigencondition, Eq. (23a) or (23b), is also in a generalized form; it is reduced for nine different combinations of the boundary conditions of the first, second, and third kinds and is presented in Table 2. The following notations are used in Table 2: $\bar{\gamma}=\gamma b$, $\bar{\eta}=\eta(c-b)$, $Bi_1=h_1b/k_{1y}$, $Bi_2=h_2(c-b)/k_{2y}$, and assuming R to be the contact resistance for a unit area, $R_b=Rk_{1y}/b$, $R_c=Rk_{2y}/(c-b)$.

4. Temperature solution

Following the identification of functions and parameters in the definition of Green's function, Eq. (9), then Eq. (13) provides the temperature solution for a two-layer body with homogeneous boundary conditions as

Table 1
Solution coefficients with contact resistance for $Y_1=A\cos(\gamma y)+B\sin(\gamma y)$

Case	A	B	C	D
(a) *when* $Y_2=C\cos(\eta y)+D\sin(\eta y)$				
Y1J[a]	0	1	$\sin(\gamma b)\cos(\eta b)-(\gamma/\eta)\times(k_{1y}/k_{2y})\cos(\gamma b)\sin(\eta b)+k_{1y}R\gamma\cos(\gamma b)\cos(\eta b)$	$\sin(\gamma b)\sin(\eta b)+(\gamma/\eta)\times(k_{1y}/k_{2y})\cos(\gamma b)\cos(\eta b)+k_{1y}R\gamma\cos(\gamma b)\sin(\eta b)$
Y2J	1	0	$\cos(\gamma b)\cos(\eta b)+(\gamma/\eta)\times(k_{1y}/k_{2y})\sin(\gamma b)\sin(\eta b)-k_{1y}R\gamma\sin(\gamma b)\cos(\eta b)$	$\cos(\gamma b)\sin(\eta b)-(\gamma/\eta)\times(k_{1y}/k_2)\sin(\gamma b)\cos(\eta b)-k_{1y}R\gamma\sin(\gamma b)\sin(\eta b)$
Y3J	1	$h_1/k_{1y}\gamma$	$\cos(\eta b)[\cos(\gamma b)+(h_1/k_{1y}\gamma)\times\sin(\gamma b)]+[k_{1y}R\gamma\cos(\eta b)-(k_{1y}/k_{2y})(\gamma/\eta)\sin(\eta b)]\times[(h_1/k_{1y}\gamma)\cos(\gamma b)-(\sin(\gamma b)]$	$\sin(\eta b)[\cos(\gamma b)+(h_1/k_{1y}\gamma)\times\sin(\gamma b)]+[k_{1y}R\gamma\sin(\eta b)+(k_{1y}/k_{2y})(\gamma/\eta)\cos(\eta b)]\times[(h_1/k_{1y}\gamma)\cos(\gamma b)-\sin(\gamma b)]$
(b) *When* $Y_2=\bar{C}\cos[\eta(y-b)]+\bar{D}\sin[\eta(y-b)]$				
Y1J[a]	0	1	$\sin(\gamma b)+k_{1y}R\gamma\cos(\gamma b)$	$(\gamma/\eta)(k_{1y}/k_{2y})\cos(\gamma b)$
Y2J	1	0	$\cos(\gamma b)-k_{1y}R\gamma\sin(\gamma b)$	$-(\gamma/\eta)(k_{1y}/k_2)\sin(\gamma b)$
Y3J	1	$(h_1/k_{1y}\gamma)$	$\cos(\gamma b)+h_1/(k_{1y}\gamma)\sin(\gamma b)+k_{1y}R\gamma[(h_1/k_{1y}\gamma)\cos(\gamma b)-\sin(\gamma b)]$	$(k_{1y}/k_{2y})(\gamma/\eta)\times[(h_1/k_{1y}\gamma)\cos(\gamma b)-\sin(\gamma b)]$

[a] J stands for a boundary condition of the first, second, or third kind at $y=c$.

Table 2
Eigenconditions for Y11, Y12, Y13, Y21, Y22, Y23, Y31, Y32, and Y33[a]

Case	Eigencondition
Y11	$\cot(\bar{\eta}) = -\left(\frac{c-b}{b}\right)\left(\frac{\bar{\gamma}}{\bar{\eta}}\right)\left(\frac{k_{1y}}{k_{2y}}\right)\frac{\cot\left(\bar{\gamma}\right)}{1+R_b\bar{\gamma}\cot(\bar{\gamma})}$
Y12	$\tan(\bar{\eta}) = \left(\frac{c-b}{b}\right)\left(\frac{\bar{\gamma}}{\bar{\eta}}\right)\left(\frac{k_{1y}}{k_{2y}}\right)\frac{\cot\left(\bar{\gamma}\right)}{1+R_b\bar{\gamma}\cot(\bar{\gamma})}$
Y13	$\frac{\bar{\eta}\tan(\bar{\eta}) - Bi_2}{(Bi_2 - R_c\bar{\eta}^2)\tan(\bar{\eta}) + \bar{\eta}(1+R_cBi_2)} = \left(\frac{c-b}{b}\right)\left(\frac{\bar{\gamma}}{\bar{\eta}}\right)\left(\frac{k_{1y}}{k_{2y}}\right)\cot(\bar{\gamma})$
Y21	$\cot(\bar{\eta}) = \left(\frac{c-b}{b}\right)\left(\frac{\bar{\gamma}}{\bar{\eta}}\right)\left(\frac{k_{1y}}{k_{2y}}\right)\frac{\tan(\bar{\gamma})}{1-R_b\bar{\gamma}\tan(\bar{\gamma})}$
Y22	$\tan(\bar{\eta}) = -\left(\frac{c-b}{b}\right)\left(\frac{\bar{\gamma}}{\bar{\eta}}\right)\left(\frac{k_{1y}}{k_{2y}}\right)\frac{\tan(\bar{\gamma})}{1-R_b\bar{\gamma}\tan(\bar{\gamma})}$
Y23	$\frac{\bar{\eta}\tan(\bar{\eta}) - Bi_2}{(Bi_2 - R_c\bar{\eta}^2)\tan(\bar{\eta}) + \bar{\eta}(1+R_cBi_2)} = -\left(\frac{c-b}{b}\right)\left(\frac{\bar{\gamma}}{\bar{\eta}}\right)\left(\frac{k_{1y}}{k_{2y}}\right)\tan(\bar{\gamma})$
Y31	$\cot(\bar{\eta}) = \left(\frac{c-b}{b}\right)\left(\frac{\bar{\gamma}}{\bar{\eta}}\right)\left(\frac{k_{1y}}{k_{2y}}\right)\frac{\bar{\gamma}\tan(\bar{\gamma}) - Bi_1}{(Bi_1 - R_b\bar{\gamma}^2)\tan(\bar{\gamma}) + \bar{\gamma}(1+R_bBi_1)}$
Y32	$\tan\bar{\eta} = -\left(\frac{c-b}{b}\right)\left(\frac{\bar{\gamma}}{\bar{\eta}}\right)\left(\frac{k_{1y}}{k_{2y}}\right)\frac{\bar{\gamma}\tan(\bar{\gamma}) - Bi_1}{(Bi_1 - R_b\bar{\gamma}^2)\tan(\bar{\gamma}) + \bar{\gamma}(1+R_bBi_1)}$
Y33	$\frac{\bar{\eta}\tan\left(\bar{\eta}\right) - Bi_2}{Bi_2\tan(\bar{\eta}) + \bar{\eta}} = -\left(\frac{c-b}{b}\right)\left(\frac{\bar{\gamma}}{\bar{\eta}}\right)\left(\frac{k_{1y}}{k_{2y}}\right)\frac{\bar{\gamma}\tan(\bar{\gamma}) - Bi_1}{(Bi_1 - R_b\bar{\gamma}^2)\tan(\bar{\gamma}) + \bar{\gamma}(1+R_bBi_1)}$

[a] The parameters γ and η are related by the relations $\gamma^2 = \lambda^2/\alpha_{1y} - (r_1^2\beta^2 + s_1^2\nu^2)$ and $\eta^2 = \lambda^2/\alpha_{2y} - (r_2^2\beta^2 + s_2^2\nu^2)$ where $r_i = (k_{ix}/k_{iy})^{1/2}$, $s_i = (k_{iz}/k_{iy})^{1/2}$ for $i = 1$ or 2, and R = contact resistance. Notations: $\bar{\gamma} = \gamma b$, $\bar{\eta} = \eta(c-b)$, $Bi_1 = h_1 b/k_{1y}$, $Bi_2 = h_2(c-b)/k_{2y}$, $R_b = Rk_{1y}/b$, $R_c = Rk_{2y}/(c-b)$, and R is defined so that $(T_1 - T_2)|_{y=b}/R = -k_{1y}(\partial T/\partial y)|_{y=b}$.

$$
\begin{aligned}
&T_i(x,y,z,t)\\
&= \sum_{p=1}^{\infty}\sum_{m=1}^{\infty}\sum_{n=1}^{\infty}\frac{X_m(x)Z_n(z)Y_{i,mnp}(y)\exp(-\lambda_{mnp}^2 t)}{N_{x,m}N_{y,mnp}N_{z,n}}\\
&\quad\times\int_{z=0}^{d}\int_{x=0}^{a}\left[\int_{y=0}^{b}\rho_1 c_{p1}Y_{1,mnp}(y')T_1(x',y',z',0)\,\mathrm{d}y'\right.\\
&\quad\left.+\int_{y=b}^{c}\rho_2 c_{p2}Y_{2,mnp}(y')T_2(x',y',z',0)\,\mathrm{d}y'\right]\\
&\quad\times X_m(x')Z_n(z')\mathrm{d}x'\,\mathrm{d}z' + \sum_{p=1}^{\infty}\sum_{m=1}^{\infty}\sum_{n=1}^{\infty}\frac{X_m(x)Z_n(z)Y_{i,mnp}(y)}{N_{x,m}N_{y,mnp}N_{z,n}}\\
&\quad\times\int_{\tau=0}^{t}\exp[-\lambda_{mnp}^2(t-\tau)]\\
&\quad\times\int_{z=0}^{d}\int_{x=0}^{a}\left[\int_{y=0}^{b}Y_{1,mnp}(y')g_1(x',y',z',\tau)\,\mathrm{d}y'\right.\\
&\quad\left.+\int_{y=b}^{c}Y_{2,mnp}(y')g_2(x',y',z',\tau)\,\mathrm{d}y'\right]X_m(x')Z_n(z')\,\mathrm{d}x'\,\mathrm{d}z'\,\mathrm{d}\tau
\end{aligned}
\tag{25}
$$

for $i = 1$ or 2. The functions $X_m(x)$, $Z_n(z)$ are solutions of the differential equations, given by Eqs. (3a) and (3b), that are obtainable in a standard manner. Eq. (14a) yields the function $Y_{1,mnp}(y)$ after replacing γ by γ_{mnp}. Also, Eq. (24) describes the function $Y_{2,mnp}(y)$ once η is replaced by η_{mnp}.

It is instructive to examine the solutions given by Eq. (25) for multiplicative variations in the initial temperature and the volumetric energy generation. Let functions $T_1(x,y,z,0)$, $T_2(x,y,z.0)$, $g_1(x,y,z,t)$, and $g_1(x,y,z,t)$ be separable and described by

$$T_1(x,y,z,0) = T_{10}T_{1x}(x)T_{1y}(y)T_{1z}(z),$$

$$T_2(x,y,z.0) = T_{20}T_{2x}(x)T_{2y}(y)T_{2z}(z),$$

$$g_1(x,y,z,t) = g_{10}g_{1x}(x)g_{1y}(y)g_{1z}(z)g_{1t}(t),$$

$$g_2(x,y,z,t) = g_{20}g_{2x}(x)g_{2y}(y)g_{2t}(z)g_{2t}(t).$$

Then, the temperature given by Eq. (25) can be written as

$$
\begin{aligned}
&T_i(x,y,z,t)\\
&=\sum_{p=1}^{\infty}\sum_{m=1}^{\infty}\sum_{n=1}^{\infty}\frac{X_m(x)Z_n(z)Y_{i,mnp}(y)\exp(-\lambda_{mnp}^2 t)}{N_{x,m}N_{y,mnp}N_{z,n}}\\
&\times\left[T_{10}\rho_1 c_{p1}\int_{x'=0}^{a}X_m(x')T_{1x}(x')\,\mathrm{d}x'\int_{y'=0}^{b}Y_{1,mnp}(y')\right.\\
&\times T_{1y}(y')\,\mathrm{d}y'\int_{z'=0}^{d}Z_n(z')T_{1z}(z')\,\mathrm{d}z'+T_{20}\rho_2 c_{p2}\\
&\times\int_{x'=0}^{a}X_m(x')T_{2x}(x')\,\mathrm{d}x'\int_{y'=b}^{c}Y_{2,mnp}(y')T_{2y}(y')\,\mathrm{d}y'\\
&\times\left.\int_{z'=0}^{d}Z_n(z')T_{2z}(z')\,\mathrm{d}z'\right]+\sum_{p=1}^{\infty}\sum_{m=1}^{\infty}\sum_{n=1}^{\infty}\frac{X_m(x)Z_n(z)Y_{i,mnp}(y)}{N_{x,m}N_{y,mnp}N_{z,n}}\\
&\times\int_{\tau=0}^{t}\exp[-\lambda_{mnp}^2(t-\tau)]\left[g_{10}\int_{x'=0}^{a}X_m(x')g_{1x}(x')\,\mathrm{d}x'\right.\\
&\times\int_{y'=0}^{b}Y_{1,mnp}(y')g_{1y}(y')\,\mathrm{d}y'\int_{z'=0}^{d}Z_n(z')g_{1z}(z')\,\mathrm{d}z'g_{1t}(\tau)\,\mathrm{d}\tau\\
&+g_{20}\int_{x'=0}^{a}X_m(x')g_{2x}(x')\,\mathrm{d}x'\int_{y'=b}^{c}Y_{2,mnp}(y')g_{2y}(y')\,\mathrm{d}y'\\
&\times\left.\int_{z'=0}^{d}Z_n(z')g_{2z}(z')\,\mathrm{d}z'g_{2t}(\tau)\,\mathrm{d}\tau\right]. \qquad (26)
\end{aligned}
$$

5. Computation of eigenvalues

One basic method of finding eigenvalues is to begin at the smallest reasonable value for λ, that is, at the smaller of $[\alpha_{1y}(r_1^2\beta^2+s_1^2\nu^2)]^{1/2}$ and $[\alpha_{2y}(r_2^2\beta^2+s_2^2\nu^2)]^{1/2}$, see Eqs. (6a) and (6b). Using Eq. (22) with γ and η taken from Eqs. (6a) and (6b), one can march forward, $\Delta\lambda$ at a time, searching for the eigenvalues. This method is computationally slow. Also, it can result in missing eigenvalues because, as will be shown later, the spacing between successive eigenvalues can become small, less than $\Delta\lambda$. In practice, it is possible to develop a more efficient scheme. For each eigenvalue, there are well-defined upper and lower values for λ within which only one eigenvalue is located. For every entry in Table 2, these limits are the ordered locations of the asymptotes for the right side and for the left side of each equation. The asymptotes will be located where the denominators of the right side and of the left side of an entry in Table 2 become zero. Between any two adjacent asymptotes, there is one eigenvalue. This is demonstrated by using the following quantities that approximate those in Dowding et al. [12] for an orthotropic carbon–carbon layer attached to a thin layer of mica: $a=d=10$ cm, $b=0.9$ cm, $c=1$ cm, $k_{1x}=k_{1z}=0.5$ W/cm K, $k_{1y}=0.1$ W/cm, $k_{2x}=k_{2y}=k_{2z}=0.01$ W/cm, $\rho_1 c_{p1}=2.6$ kJ/cm^3 K, $\rho_2 c_{p2}=2.4$ kJ/cm^3 K and $h_1=h_2=0$. Furthermore, it is assumed $R=0.45$ cm^2 K/W, $\beta=5\pi/a$, and $\nu=10\pi/d$.

The solid line, labeled as "right side" in Fig. 2(a), is the right side of entry 9 in Table 2 plotted as a function of λ^2. Similarly, the dash line in Fig. 2(a) shows the variation of the left side of entry 9 in Table 2. The eigenvalues are located where the solid line and the dash

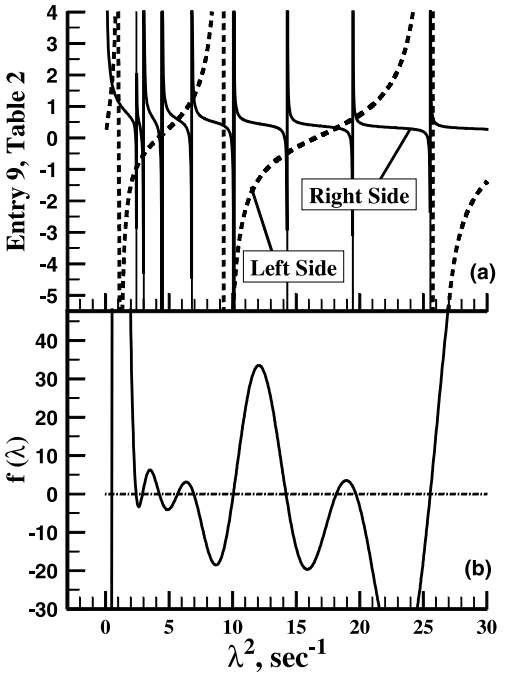

Fig. 2. (a) Right side, the solid lines, and left side, the dash lines, of entry 9 in Table 2 and (b) variation of $f(\lambda)$, Eq. (22), as a function of λ^2.

line have the same values. As an alternative scheme, one can use the zeros of the right side and left side of each eigencondition entry in Table 2, and between any two adjacent zeros there is an eigenvalue. Columns 1 and 2 in Table 3 show the locations of the right side and left side asymptotes that appear in Fig. 2(a). Each computed eigenvalue, in column 3, is located between two adjacent asymptotes. For example $\lambda^2 = 25.54791$ is between 25.54582 in column 1 and 25.75350 in column 2. Fig. 2(b) is plotted to show the zeros of function $f(\lambda)$, Eq. (22), as a function of λ. This figure demonstrates that the spacing between neighboring eigenvalues changes and can become very small; therefore, it is important to identify a bound on the location of each eigenvalue a priori. Also, it is possible for the spacing between two adjacent asymptotes to become zero.

The locations of the asymptotes are the same as the eigenvalues for individual layers. For example, the asymptotes for the right side of entry 9, in Table 2, are located when $\bar{\gamma}$ is calculated using the relation

$$(Bi_1 - R_b\bar{\gamma}^2)\tan(\bar{\gamma}) + \bar{\gamma}(1 + R_b Bi_1) = 0 \tag{27a}$$

that, when $R_b = 1/Bi_b$, can be written as

$$(Bi_1 Bi_b - \bar{\gamma}^2)\tan(\bar{\gamma}) + \bar{\gamma}(Bi_b + Bi_1) = 0. \tag{27b}$$

This is the same eigencondition for a single layer body with thickness b, with Biot number Bi_1 at $y = 0$ and Biot number $Bi_b = 1/R_b$ at $y = b$. The asymptotes for the left side are the roots of equation

$$Bi_2 \tan(\bar{\eta}) + \bar{\eta} = 0. \tag{28}$$

This is the eigencondition for a single layer body with thickness $c - b$, insulated at $y = b$ and having a Biot number $Bi_2 = h_2(c - b)/k_{2y}$ at $y = c$. The right-side/left-side asymptotes for other entries in Table 2 are obtainable in a similar manner. The location of these asymptotes is known using an explicit equation [13]. Once a bound on the location of each eigenvalue is established, a hybrid computing technique [10] provides the numerical value of that eigenvalue. The hybrid computing technique begins by using a bisection method while simultaneously computing the first and the second derivatives of function $f(\lambda)$, Eq. (22), by central differencing. After f''/f' reduces to below a prescribed limit, a second-order Newton method yields the final numerical result. The basic steps for the second-order Newton method, as described in [10], are to calculate $f_0 = f(\lambda_0)$, and then $f_1 = f'(\lambda_0)$, and $f_2 = f''(\lambda_0)$ by central differencing. The next value of λ, that is, λ_1 will be

$$\lambda_1 = \lambda_0 - \frac{f_0}{f_1} + \frac{1}{2}\frac{f_2 f_0^2/f_1}{f_2 f_0 - f_1^2}. \tag{29}$$

Typically, 4 to 6 bisection steps and ~2 second-order Newton steps would provide an accurate eigenvalue.

Table 3
Locations of the eigenvalues and the right-/left-side asymptotes in Fig. 2

Right side	Left side	Eigenvalues
–	0.051404[a]	0.50961
–	1.07950	2.40929
2.43082	–	2.91648
3.01705	–	4.23901
4.44565	–	5.67551
6.79527	–	6.94996
–	9.30416	10.06049
10.07829	–	14.20126
14.29730	–	18.15974
19.45305	–	19.69501
25.54582	–	25.54791
–	25.75350	–

[a] Starting value.

6. Numerical examples

Numerical examples are selected to demonstrate the scope of this solution method. The first example studies one-dimensional transient heat conduction and then is extended to three- dimensional heat conduction in the second and the third examples. The main emphases in these examples are to demonstrate the use of the above analysis and to give insight into efficient computation of the temperature and heat fluxes.

Example 1. This example is one-dimensional with convection to an ambient temperature of T_∞ at both ends and a very large, but of short duration, heat flux at $y = 0$. The initial temperature is also equal to T_∞. The selected parameters are: $b = 0.25$ cm, $c = 0.5$ cm, $k_{1y} = 0.1$ W/cm K, $k_{2y} = 0.7$ W/cm K, $h_1 = 0.1$ W/cm^2 K, $h_2 = 0.3$ W/cm^2 K, $\rho_1 c_{p1} = 3$ J/cm^3 K, and $\rho_2 c_{p2} = 4$ J/cm^3 K. Region 1 has a lower thermal diffusivity. Perfect contact exists between regions 1 and 2; see Fig. 1. The entire surface at y = 0 is irradiated at the rate of $q_1 = 10$ kW/cm^2 for a duration of $t_o = 1$ ms. The solution is then written, using Eq. (25) for homogeneous boundary conditions and initial condition while accounting for the surface heat flux by using $g_1(x,t) = q_1(t)\delta(y - 0)$ in Region 1 by, as

$$\begin{aligned} T_i(y,t) - T_\infty &= \sum_{p=1}^{\infty} \frac{Y_{i,p}(y)}{N_p} \int_{\tau=0}^{t} \exp[-\lambda_p^2(t-\tau)] \\ &\quad \times \int_{y=0}^{b} Y_{1,p}(y') q_1(\tau)\delta(y' - 0)\,\mathrm{d}y'\,\mathrm{d}\tau \\ &= q_1 \sum_{p=1}^{\infty} \frac{Y_{i,p}(0)Y_{i,p}(y)}{\lambda_p^2 N_p} \Phi_p(t, t_o), \end{aligned} \tag{30a}$$

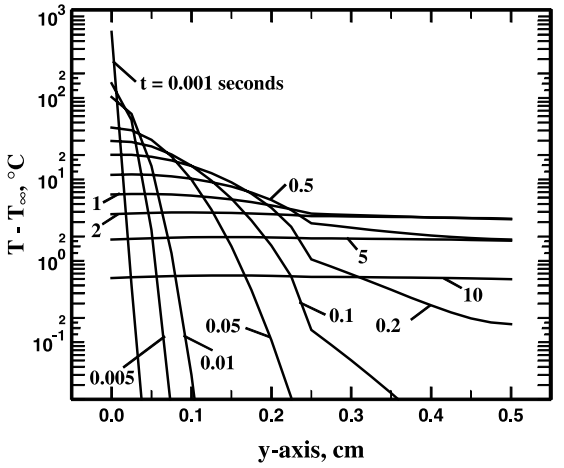

Fig. 3. One-dimensional temperature solution for a two-layer body in Example 1.

where

$$\Phi_p(t,t_o)=\begin{cases}1-\exp(-\lambda_p^2 t) & \text{when } t\leqslant t_o,\\ \exp[-\lambda_p^2(t-t_o)]-\exp(-\lambda_p^2 t) & \text{when } t>t_o.\end{cases} \tag{30b}$$

Expressions for $Y_{1,p}(y)$ and $Y_{2,p}(y)$ are taken from Eqs. (14a) and (24) and Y3J entry in Table 1b, as

$$Y_{1,p}(y)=\cos(\gamma_p y)+\left(\frac{h_1}{k_{1y}\gamma_p}\right)\sin(\gamma_p y), \tag{31a}$$

$$Y_{2p}=\bar{C}_p\cos[\eta_p(y-b)]+\bar{D}_p\sin[\eta_p(y-b)]. \tag{31b}$$

where

$$\bar{C}_p=\cos(\gamma_p b)+(h_1/k_{1y}\gamma_p)\sin(\gamma_p b)+k_{1y}R\gamma_p[(h_1/k_{1y}\gamma_p)\cos(\gamma_p b)-\sin(\gamma_p b)] \tag{32a}$$

$$\bar{D}_p=(k_{1y}/k_{2y})(\gamma_p/\eta_p)[(h_1/k_{1y}\gamma_p)\cos(\gamma_p b)-\sin(\gamma_p b)] \tag{32b}$$

The eigenvalues are obtained numerically using the entry 9 in Table 2 after setting $\beta=0$ and $v=0$ to get $\gamma_p^2=\lambda_p^2/\alpha_{1y}$ and $\eta_p^2=\lambda_p^2/\alpha_{2y}$. In one-dimensional problems, all eigenvalues are real. The computed first six eigenvalues, λ_1–λ_6, are: 0.4661446, 1.477978, 3.381259, 5.001021, 6.148723, and 8.031121. The corresponding values of the norms, N_1–N_6, are: 1.855151, 0.5194274, 0.4440894, 0.7692402, 0.5480879, and 0.4300197.

Fig. 3 shows the temperature solution as a function of the y-coordinate for different times between 0.001 and 10 s. As expected, the convergence is fast when $t>t_o$; however, when $t=0.001$ s, the series solution sufficiently converges when the number of terms exceeds 1000. However, at small times, modeling Region 1 as a semi-infinite body dramatically reduces the number of terms. Numerical values for the semi-infinite solution and composite solution with 100 terms are given in Table 4 where the temperature is computed at different times up to 0.1 s and for different locations from $y=0$ to b. Since iteration is not needed to compute the eigenvalues [13], they are acquired within a fraction of a second on a personal computer. The numbers inside parentheses are the temperatures obtained assuming Region 1 to be a semi-infinite solid irradiated at $y=0$. Since q_1 and h_1 are constants, the solution in the semi-infinite region using the function

$$U(y,t)=\frac{q_1}{h_1}\left[\operatorname{erfc}\left(y/\sqrt{4\alpha_{1y}t}\right)+\exp(h_1 y/k_{1y}+\alpha_{1y}th_1^2/k_{1y}^2)\times\operatorname{erfc}\left(y/\sqrt{4\alpha_{1y}t}+\sqrt{\alpha_{1y}t}h_1/k_{1y}\right)\right] \tag{33a}$$

taken from 11, Eq. (6.29), and superposition is

$$T(y,t)-T_\infty=\begin{cases}U(y,t) & \text{when } t\leqslant t_o,\\ U(y,t)-U(y,t-t_o) & \text{when } t>t_o.\end{cases} \tag{33b}$$

A comparison between the two solutions shows that the solution for a semi-infinite body departs from a two-layer solution at, $y=b$, when $t\approx 0.05$ s; this corresponds to $\alpha_1 t/b^2\approx 0.027$. The surface temperature is very accurately predicted until a dimensionless time 4 times as large, or until 0.2s in this case; the computed temperature is 20.0143 °C while the two-layer solution yields 20.0125 °C. Hence if the heated surface temperature is of primary interest, it can be computed using the semi-infinite solution given above and then the composite solution thereafter with less than six terms in the summation. When $t=0.1$ s, only six eigenvalues are needed to provide values within 0.0012 °C at any

location and the accuracy improves as t increases and t increases.

Example 2. In Example 1, it is shown that the series convergence is poor when $\Phi_p(t,t_o) = 1 - \exp(-\lambda_p^2 t)$. To study this effect and the influence of spatial functions, the transient solution is used to compute temperature along the y-axis, see Fig. 1, as time becomes large. In this study, $a = d = 1$ cm and the surfaces at $x = 0$, a and $z = 0$, d are insulated. It is assumed that all properties and dimensions are the same as those in Example 1 except there is a prescribed uniform heat flux over the $y = 0$ surface when $0 \leqslant x \leqslant a_1$ and $0 \leqslant z \leqslant d_1$. The temperature solution has the following form:

$$T_i(y,t) - T_\infty = q_1 \sum_{p=1}^{\infty}\sum_{m=1}^{\infty}\sum_{n=1}^{\infty} V_m(x)W_n(z) \times \frac{Y_{i,p}(0)Y_{i,p}(y)[1-\exp(-\lambda_p^2 t)]}{\lambda_p^2 N_p}, \quad (34)$$

wherein the functions $V_m(x)$ and $W_n(z)$ are

$$U_m(x) = \begin{cases} a_1/a & \text{when } m = 0, \\ \frac{2}{m\pi}\cos(m\pi x/a)\sin(m\pi a_1/a) & \text{when } m > 0, \end{cases} \quad (35a)$$

$$W_n(z) = \begin{cases} d_1/d & \text{when } n = 0, \\ \frac{2}{n\pi}\cos(n\pi x/a)\sin(n\pi a_1/a) & \text{when } n > 0. \end{cases} \quad (35b)$$

The temperature solution, Eq. (34), approached steady-state solution as $t \to \infty$. The solid lines in Fig. 4(a) show the computed near-steady-state data when $a_1/a = d_1/d = 0.2$, 0.5, 0.8, and 1. The discrete data are the standard one-dimensional steady-state temperature solution. As expected, when $a_1/a = d_1/d = 1$, the corresponding solid line and the discrete data are nearly identical. The three-dimensional computations are performed using maximum values for indices m, n, and p equal to 30, 30, and 50, respectively.

To demonstrate the convergence rate for the steady-state case, when $a_1/a = d_1/d = 1$, the absolute value of the deviation of the series solution from the exact solution, ε, is computed and plotted in Fig. 4(b) wherein ε is defined by the relation

$$\varepsilon = [(T - T_\infty)|_{\text{series}} - (T - T_\infty)|_{\text{exact}}]/(T - T_\infty)|_{\text{exact}}. \quad (36)$$

Based on the data in Fig. 4(b), for a high degree of accuracy while keeping the number of terms small, it is important to find techniques such as time partitioning [Chapter 5]11, to accelerate the convergence.

Example 3. This example demonstrates the peculiarities of a three-dimensional transient solution. To maintain the brevity of the presentation, input data in Example 1 are slightly modified. Furthermore, it is hypothesized that the surface at $x = a$ is cooled by a fluid so that the $x = a$ surface remains at a constant temperature equal to the ambient temperature T_∞; however, the surfaces at $x = 0$, $z = 0$, and $z = d$ remain insulated. The heat transfer coefficients h_1 and h_2 remain at those values specified in Example 1. The temperature field becomes three-dimensional assuming the $y = 0$ surface receives heat flux over a small area bounded by bounded by the

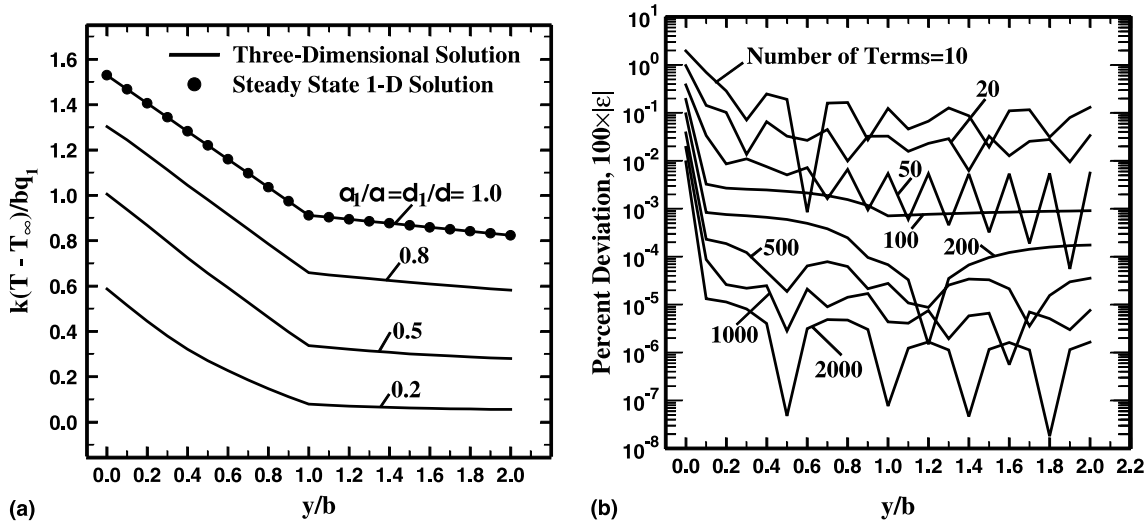

Fig. 4. (a) Steady-state dimensionless temperature solution from Eq. (34) along y-axis for different heated areas over $y = 0$ surface, when $a_1/a = d_1/d$, see Example 2. (b) Absolute value of the deviation ε, Eq. (36), using 10, 20, 50, 100, 200, 500, 1000, and 2000 terms in the one-dimensional series solution, Eq. (34), when $a_1/a = d_1/d = 1$.

lines $x = 0, a_1$ and $z = 0, d_1$ as in Example 2. Eq. (34) in Example 2 would describe the temperature distribution if

$$V_m(x) = 2\cos[(m+1/2)\pi x/a]\sin[(m+1/2)\pi a_1/a] \Big/ [(m+1/2)\pi]. \quad (37)$$

When $a_1 = 0.5a$ and $d_1 = 0.5d$, the dimensionless temperature $k(T - T_\infty)/bq_1$ along a line, with coordinates $x = 0$ and $z = 0$, is plotted as a function of y in Fig. 5. Each line in the figure is for a different Fourier number, $Fo = \alpha_{1y}t/b^2$. Fig. 5 is prepared in a similar manner, except the data are plotted as a function of y when $x = 0$ and $z = d_1$. Figs. 5 and 6 clearly show the three-dimensional effect, as temperatures in Fig. 6 are less than those shown in Fig. 5. This example reveals some computational peculiarities when β_m and v_n are large and η_{mnp} is imaginary. A discussion is in the following section.

7. Remarks

As stated earlier, the computation of eigenvalues requires extreme care. Indeed, the computation of temperature also requires extreme care when a spatial eigenvalue γ or η becomes imaginary. In this case, since $\alpha_{1y} < \alpha_{2y}$, then η_{mnp} can become imaginary when β_m and/or v_n are larger than 1. At large β_m and/or v_n values, the functions $\sin(\eta_{mnp}y)$ and $\cos(\eta_{mnp}y)$ become $-\sinh(|\eta_{mnp}|y)/\mathrm{i}$ and $\cosh(|\eta_{mnp}|y)$ as η_{mnp} becomes imaginary; therefore, these functions grow exponentially and can produce undesirable round-off errors. As demonstrated in Aviles-Ramos et al. [9], the terms with imaginary

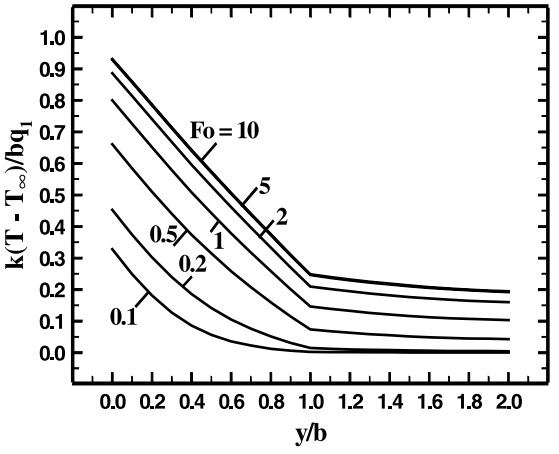

Fig. 5. Temperature, in Example 3, as a function of y/b when $x = 0$ and $z = 0$ for different Fourier numbers $\alpha_{1y}t/b^2$.

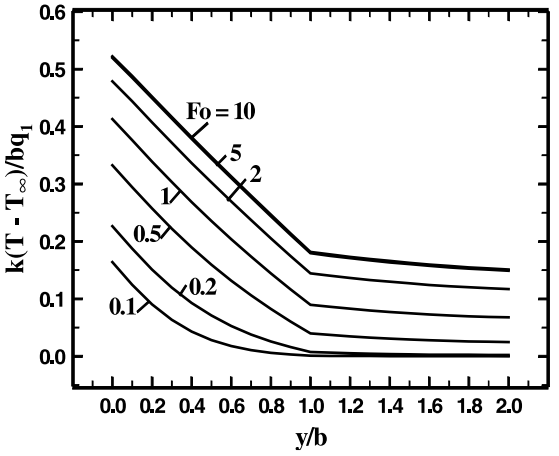

Fig. 6. Temperature, in Example 3, as a function of y/b when $x = 0$ and $z = 0.5d$ for different Fourier numbers $\alpha_{1y}t/b^2$.

Table 4
Computed temperature, $(T - T_\infty)$ °C, in Region 1 and a comparison with a solution for a semi-infinite body[a]

y (cm)	t (s)				
	0.001	0.005	0.01	0.05	0.1
0.00	574.8736 (648.1511)	150.5034 (150.5034)	102.4516 (102.4516)	43.11266 (43.11266)	29.52803 (29.52803)
0.05	−0.946044 (0.000000)	2.394879 (2.394879)	14.52021 (14.52021)	30.45890 (30.45890)	25.33503 (25.33503)
0.10	−0.786541 (0.000000)	0.000013 (0.000013)	0.039863 (0.039863)	9.908667 (9.908667)	14.66315 (14.66325)
0.15	−0.613663 (0.000000)	0.000000 (0.000000)	0.000002 (0.000002)	1.501637 (1.501638)	5.776373 (5.777962)
0.20	−0.401243 (0.000000)	0.000000 (0.000000)	0.000000 (0.000000)	0.106381 (0.106409)	1.537475 (1.555826)
0.25	−0.160965 (0.000000)	0.000000 (0.000000)	0.000000 (0.000000)	0.001742 (0.003531)	0.141438 (0.286766)

[a] The numbers inside parentheses are solutions for a semi-infinite body.

spatial eigenvalues must be included in the solution; otherwise the computations would yield erroneous results. The condition exists when $\alpha_{1y} > \alpha_{2y}$ and the spatial eigenvalue γ_{mnp} is imaginary. In this latter case, the remedial steps are simple as the entries for A, and B in Table 1(a) or (b) can be scaled down using a factor, i.e., $\exp[-|\gamma_{mnp}|b]$.

When η_{mnp} is imaginary, the computation of eigenvalues requires some attention. However, the numerical computation of temperature, using the data for this example, also produced severe numerical errors when $y > b$, mainly due to standard numerical truncation within the computer processor. The error becomes severe when calculating $Y_{2,mnp}(y)$ and its contribution to the norm. To overcome problems associated with the truncation errors, the method of computing $Y_{2,mnp}(y)$, when η_{mnp} is imaginary, should be modified. Based on Eq. (21), coefficients $\bar{C}$ and $\bar{D}$ from Table 1(b), entry Y3J, are related, therefore, when $\eta_{mnp} = \mathrm{i}|\eta_{mnp}|$, here $\mathrm{i} = \sqrt{-1}$, they are

$$\bar{C}_{mnp} = \left[\cos(\gamma_{mnp}b) + \left(\frac{h_1}{k_{1y}\gamma_{mnp}}\right)\sin(\gamma_{mnp}b)\right] + k_{1y}R\gamma_{mnp}\left[\left(\frac{h_1}{k_{1y}\gamma_{mnp}}\right)\cos(\gamma_{mnp}b) - \sin(\gamma_{mnp}b)\right] \tag{38a}$$

and

$$\bar{D}_{mnp} = \mathrm{i}\bar{C}_{mnp}\frac{|\eta_{mnp}|\tanh[|\eta_{mnp}|(c-b)] + h_2/k_{2y}}{|\eta_{mnp}| + (h_2/k_{2y})\tanh[|\eta_{mnp}|(c-b)]}. \tag{38b}$$

Then, Eq. (14b) following substitution for D and other appropriate algebraic steps yields

$$Y_{2,mnp}(y) = \bar{C}_{mnp}\exp[-|\eta_{mnp}|(y-b)] + \bar{C}_{mnp}\Psi(|\eta_{mnp}|)\sinh[|\eta_{mnp}|(y-b)], \tag{39a}$$

where

$$\Psi(|\eta_{mnp}|) = \left[1 - \frac{|\eta_{mnp}|\tanh[|\eta_{mnp}|(c-b)] + h_2/k_{2y}}{|\eta_{mnp}| + (h_2/k_{2y})\tanh[|\eta_{mnp}|(c-b)]}\right] \tag{39b}$$

Clearly, the term $\bar{C}$ is real and has a finite numerical value and $\exp[-|\eta_{mnp}|(y-b)]$ varies between 0 and 1 as $|\eta_{mnp}|$ increases, since $y > b$. Moreover, the term $\Psi(|\eta_{mnp}|)\sinh[|\eta_{mnp}|(y-b)]$ rapidly becomes small as $|\eta_{mnp}|b$ becomes large, e.g., $|\eta_{mnp}|b > 10$. As shown above, when $y > b$, $Y_{2,mnp}(y) \to 0$ as $|\eta_{mnp}| \to \infty$; a desirable feature to achieve convergence. In general, Eq. (39a) should be used when η_{mnp} is imaginary.

8. Conclusion

There are a few items one must consider when dealing with problems of this type. In general, the spatial eigenvalues for the solution perpendicular to the layers can become imaginary within the region with higher thermal diffusivity. Usually, for each set of β_m and v_n, only the first few eigenvalues are imaginary and their numbers and magnitudes increase as the number of terms in x- and z-direction solutions increases. This phenomenon can cause the magnitude of the function $f(\lambda)$ to become very large or very small. Also, as described earlier, care must be exercised when computing the function $Y_{2,mnp}(y)$ when η_{mnp} is imaginary. Usually, it is best to arrange the coordinate system so that a layer

with the largest thermal diffusivity is Region 1, between $y = 0$ to b. However, to study the behavior of this solution technique, Region 1 in Examples 1–3 has the smaller thermal diffusivity.

In principle, to provide the best accuracy at very small or very large time, a convergence-accelerating scheme, such as time partitioning is needed. For instance, when heating begins at $y = 0$ surface, one can consider Region 1 as a semi-infinite solid when $\alpha_1 t/b^2 \leqslant 0.027$ and obtain an accurate solution using time partitioning, as described in Example 1. A similar procedure may be used when heating begins at the $y = c$ surface. In this case, Region 2 may be considered as a semi-infinite body when $\alpha_2 t/(c-b)^2 \leqslant 0.027$. However, to perform time partitioning, when there is an abrupt temperature change at the interface, where $y = b$, a different equation is needed. The temperature solution in an infinite body having two layers, introduced in 7, is suitable for a time-partitioning task. When there are two or more nonhomogeneous boundary conditions, time partitioning can be used for each surface separately. There are other challenges remaining that deserve separate studies.

Acknowledgements

This work was supported in part by Sandia National Laboratories of Albuquerque, NM.

References

[1] C.W. Tittle, Boundary value problems in composite media, J. Appl. Phys. 36 (1965) 1486–1488.

[2] J. Padovan, Generalized Sturm–Liouville procedure for composite domain anisotropic transient heat conduction problems, AIAA J. 12 (1974) 1158–1160.

[3] M.N. Ozisik, Heat Conduction, second ed., Wiley, New York, 1993.

[4] H. Salt, Transient conduction in a two-dimensional composite slab – I. Theoretical development of temperature modes, Int. J. Heat Mass Transfer 26 (1983) 1611–1616.

[5] H. Salt, Transient conduction in two-dimensional composite slab – II. Physical interpretation of temperature modes, Int. J. Heat Mass Transfer 26 (1983) 1617–1623.

[6] M.D. Mikhailov, M.N. Ozisik, Transient conduction in a three-dimensional composite slab, Int. J. Heat Mass Transfer 29 (1986) 340–342.

[7] Ling Yan, A. Haji-Sheikh, J.V. Beck, Thermal characteristics of two-layered bodies with embedded thin-film heat source, ASME J. Electron. Packaging 115 (1993) 276–283.

[8] F. de Monte, Transient heat conduction in one-dimensional composite slab. A 'natural' analytical approach, Int. J. Heat Mass Transfer 43 (2000) 3607–3616.

[9] C. Aviles-Ramos, A. Haji-Sheikh, J.V. Beck, Exact solution of heat conduction in composites and application to inverse problems, ASME J. Heat Transfer 120 (1998).

[10] C. Aviles-Ramos, K.T. Harris, A. Haji-Sheikh, A hybrid root finder, in: B. Bertram, C. Constanda, A. Struthers (Eds.), Integral Methods in Science and Engineering (1998), Chapman & Hall/CRC Press, London, UK, 2000, pp. 41–450.

[11] J.V. Beck, K. Cole, A. Haji-Sheikh, B. Litkouhi, Heat Conduction Using Green's Functions, Hemisphere, Washington, DC, 1992.

[12] K.J. Dowding, J.V. Beck, B.F. Blackwell, Estimation of directional-dependent thermal properties in a carbon–carbon composite, Int. J. Heat Mass Transfer 39 (1996) 3157–3164.

[13] A. Haji-Sheikh, J.V. Beck, An efficient method of computing eigenvalues in heat conduction, Numer. Heat Transfer (B) 38 (2000) 133–156.